PHYSICS OF FLUIDS VOLUME 10, NUMBER 10 OCTOBER 1998

Asymptotic spreading rate of initially compressible jets—experiment and analysis

K. B. M. Q. Zaman
NASA Lewis Research Center, Cleveland, Ohio 44135

(Received 4 March 1998; accepted 2 July 1998)

Experimental results for the spreading and centerline velocity decay rates for round, compressible jets, from a convergent and a convergent-divergent nozzle, are presented. The spreading rate is determined from the variation of streamwise mass flux obtained from Pitot probe surveys. Results for the far asymptotic region show that both spreading and centerline velocity decay rates, when nondimensionalized by parameters at the nozzle exit, decrease with increasing "jet Mach number" M_J. Dimensional analysis with the assumption of momentum conservation, together with compressible flow calculations for the conditions at the nozzle exit, predict this Mach number dependence well. The analysis also demonstrates that an increase in the "potential core length" of the jet occurring with increasing M_J, a commonly observed trend, is largely accounted for simply by the variations in the density and static pressure at the nozzle exit. The effect of decreasing mixing efficiency with increasing compressibility is inferred to contribute only partially to the latter trend. [S1070-6631(98)01910-2]

I. INTRODUCTION

An increase in jet spreading is desired in many technological applications, and thus, methods to achieve that are the subject of numerous previous investigations. Use of vortex generators (e.g., Refs. 1 and 2), asymmetric nozzle shapes (e.g., Refs. 3–5) and controlled excitation (e.g., Refs. 6 and 7) have been among the most extensively studied techniques for this purpose. It should be recognized, however, that an increased spreading rate can be achieved only in the developing region of a jet. Regardless of the events in the developing region, all submerged jets should attain similar spreading characteristics far downstream. There, when the flow has become incompressible and the jet cross section has become round the velocity profiles are self-similar. Law of similarity dictates that a suitable quantity characterizing the jet spreading, e.g., streamwise mass flow rate, when normalized by local length and velocity scales, is a constant. Dimensional reasoning also dictates that the rate of change of the flow rate with streamwise distance becomes a constant.[8]

While a constant asymptotic slope for the jet spreading curve would be obtained under proper nondimensionalization, conventional way of nondimensionalization results in a slope that is observed to vary with jet Mach number. This observation, which is the focus of the paper, needs to be clarified first. For the problem under consideration, the practical and most convenient choice of the parameters for data nondimensionalization are those occurring at the nozzle exit. The streamwise mass flow rate (referred to here simply as "mass flux"), $\dot{m}$, is almost invariably nondimensionalized by the flux at the nozzle exit, $\dot{m}_e$. Similarly, the streamwise distance, x, is typically nondimensionalized by the nozzle diameter, d_e. Figure 1 schematically shows commonly observed data trends under these coordinates. The curve in the middle is representative of a "normal," incompressible, round jet. The developing region extends several diameters from the nozzle, as marked by the thin vertical line, after which the asymptotic state is reached that is characterized by a linear variation of the mass flux. The asymptotic slope, $\partial(\dot{m}/\dot{m}_e)/\partial(x/d_e)$, measured in many previous experiments, is found to be ~ 0.28.[6,8,9] Mixing enhancement in this jet by a suitable technique can result in a rapid increase in the fluxes, typically accompanied by a lengthening of the developing region. This is represented by the curve on the top. However, once the asymptotic state is reached the curve becomes parallel to that of the normal jet.

For initially compressible jets, on the other hand, first, it takes a longer distance to reach the asymptotic state. The length of the "potential core" is observed to increase with increasing jet Mach number, M_J. (The parameter "M_J," defined clearly in the next section, represents the Mach number at the nozzle exit had the flow expanded fully. It is used as the primary variable in the present study). Second, as will be shown clearly in the following, the asymptotic slope of the flux curve becomes smaller with increasing M_J. These trends are represented by the curve at the bottom of Fig. 1. In a similar manner, the decay rate of the centerline velocity, U_c, also exhibits a dependence on M_J. The asymptotic decay rate of U_c, when expressed as $\partial(U_e/U_c)/\partial(x/d_e)$, decreases with increasing M_J.

The apparent jet Mach number dependence of the asymptotic spreading characteristics of compressible jets is addressed in this paper. An understanding of these effects and trends is important in experimental studies dealing with mixing enhancement in order to have a clear perspective. It should also be important in turbulence modeling for compressible flows, and, perhaps, critical in numerical code validation with jet flows. It ought to be apparent that an increasing density at the nozzle exit with increasing M_J must influence the observed trends. As will be shown in the fol-

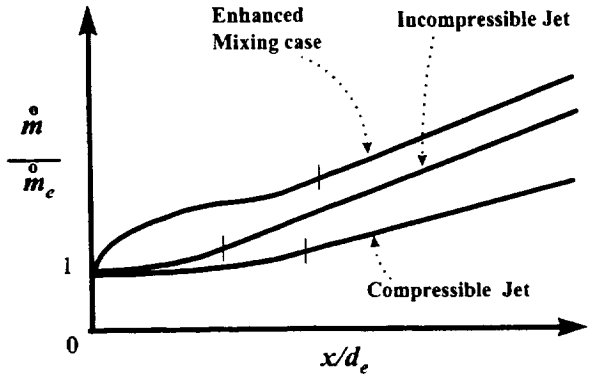

FIG. 1. Schematic of mass flux variation with streamwise distance for various conditions.

lowing, only density variation does not explain the trends fully. An unbalanced pressure at the exit (different from ambient pressure), in imperfectly expanded supersonic conditions, also comes into play. The objective of the present paper is to examine and provide an analysis for these effects.

II. EXPERIMENTAL PROCEDURE

The experiment was conducted in an open jet facility. Compressed air was supplied through one end of the plenum chamber fitted with flow conditioning units. The flow discharged through the nozzle, fitted to the other end of the plenum chamber, into the ambient of the laboratory. All jets involved "cold" flows, i.e., the total temperature was approximately constant throughout the flow. Further description of the facility can be found in Refs. 4 and 5. Data from two round nozzles are presented in this paper. One, the same as used for the "tab" studies reported in Ref. 2, is a convergent nozzle as shown in Fig. 2(a). The interior of this nozzle contracts from a diameter of 3.81 cm to the exit diameter of 1.27 cm, the contour following a third-order polynomial. The nozzle has 1.27 cm long cylindrical sections at the entrance and the exit so that the flow enters and exits axially.

The second nozzle, shown in Fig. 2(b), is a convergent-divergent one with throat and exit diameters of 2.289 and 2.54 cm, respectively. Its interior is contoured approximately following the method of characteristics for a design Mach number, $M_D = 1.58$. However, experiments with this nozzle have indicated that the flow is not completely shock free even at the design condition. From one dimensional nozzle flow analysis, based on the exit-to-throat diameter ratio, the following flow regimes are expected with this nozzle. (I) Subsonic flow throughout for $M_J < 0.57$, (II) normal shock existing in the diverging section for $0.57 < M_J < 0.79$, (III) overexpanded flow for $0.79 < M_J < 1.58$, and (IV) underexpanded flow for $1.58 < M_J$. As stated before, M_J is the Mach number at the nozzle exit had the flow expanded fully. It is given by the pressure ratio through the equation $M_J = (((p_t/p_a)^{(\gamma-1)/\gamma} - 1)[2/(\gamma-1)])^{1/2}$, where p_t is the total pressure in the plenum chamber, p_a is the ambient pressure and γ is the ratio of specific heats. Values of p_t/p_a corresponding to $M_J = 0.57$, 0.79, and 1.58 are 1.24, 1.50, and 4.11, respectively.

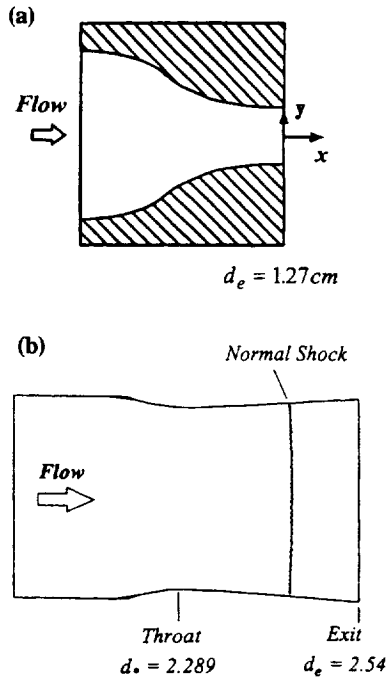

FIG. 2. Schematics of the two round nozzles, dimensions are in cm. (a) Convergent nozzle, (b) convergent-divergent nozzle.

All data were obtained by Pitot probe surveys under automated computer control. A rake of three probes was used to reduce data acquisition time. The probes were made of hypodermic needles with a 0.05 cm internal diameter and mounted on a streamlined "sting." The support structure and the traversing mechanism were sturdy enough so that there was no visually perceptible vibration or yielding of the probes under the largest dynamic load. All data were acquired far enough downstream where the flow became fully subsonic in order to avoid measurement errors typical of supersonic flows. The distribution of Pitot pressure, on the cross-sectional plane at a given x, was used to calculate the streamwise mass flux, $\dot{m} = \int\int \rho U \partial y \partial z$, where U is the streamwise velocity, ρ is the density, and y and z are the transverse coordinates. In the calculation, it was assumed that the total temperature remained the same throughout the flow field and the static pressure equaled the ambient pressure. Since the integrated flux was sensitive to small measurement errors, care had to be taken in the data acquisition. One set of pressure transducers was employed to cover regions where the centerline Mach number was greater than about 0.3. A second set of transducers with higher sensitivity was employed in regions involving lower Mach numbers. Transducer zero errors were monitored before each run. Throughout data acquisition, the plenum pressure (p_t) and ambient pressure (p_a) were monitored and data normalization was done according to current conditions. Sufficient averaging time was allowed to ensure good data repeatability.

It should be noted that there is subjectivity in the calculation of the mass flux. Because the contribution from the potential flow induced by the jet is infinite in the integration, $\dot{m} = \int\int \rho U \partial y \partial z$, a suitable criterion needs to be followed to discriminate the vortical flow from the surrounding potential

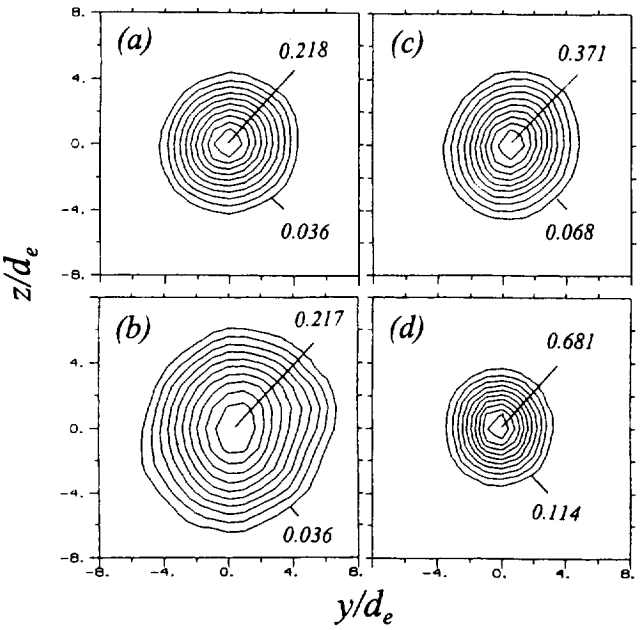

FIG. 3. Mach number contours at $x/d_e = 30$ for the convergent nozzle. "Jet Mach number" (M_J) and contour intervals are: (a) **0.97**, 0.018; (b) **1.37**, 0.018; (c) **1.63**, 0.034; (d) **1.97**, 0.057.

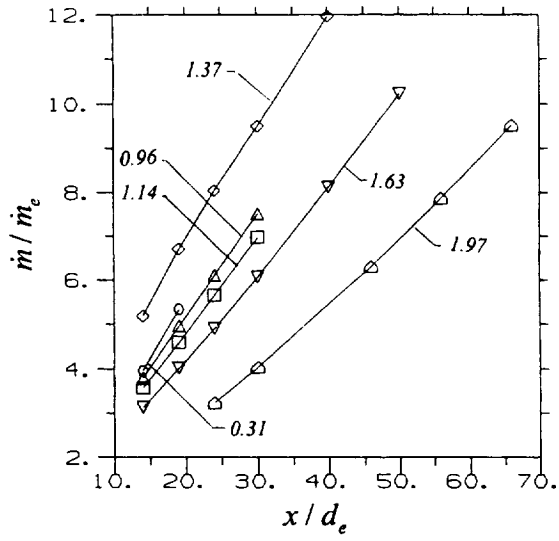

FIG. 4. Streamwise variations of normalized mass flux for indicated M_J; convergent nozzle.

flow.[6] Furthermore, Pitot probe measurements involve error on the outer periphery of the jet due to large turbulence and flow angularity. In view of these difficulties, the criterion followed here simply involved truncating the integration where the measured Mach number dropped below 1% of the local centerline Mach number. For further discussion of these considerations and limitations, the reader is referred to Refs. 5 and 10 in which preliminary results of this investigation were reported. Most of the mass flux data were repeatable within ±4%, the repeatability being better in regions of higher Mach number but worse in cases involving very low jet Mach number.

While the mass flux data were obtained for a limited number of x stations, the centerline velocity measurements were carried out in separate runs allowing for finer spatial resolution. It is worth noting that the centerline velocity U_c is a clearly defined quantity and there is no subjectivity as with the mass flux data. However, measurement is not trivial and one must account for possible misalignment of the flow and geometric axes. Some further details of the measurements can be found in Ref. 10.

III. EXPERIMENTAL RESULTS

Examples of Mach number distributions for the 1.27 cm convergent nozzle, measured thirty diameters from the exit, are shown in Fig. 3. The jet spreading for three supersonic cases is compared with that for a high subsonic case. For each case, ten contour levels are plotted, the interval being 10% of the maximum contour level that approximates the peak Mach number in the domain. This way, the jet cross-sectional boundary relative to the local peak velocity is shown. The difference in jet spreading, depending on M_J, is obvious. Here, in addition to the compressibility effect, discussed further in the following, various stages of screech cause the jet to spread differently. At $M_J = 1.37$ in Fig. 3(b), the jet undergoes the "B" (flapping) mode of screech. Under this condition the jet goes through the most pronounced spreading. At $M_J = 1.63$ in Fig. 3(c), the jet undergoes the helical "C" mode of screech and the spreading is not as much. At the highest value of M_J in Fig. 3(d), screech amplitude is negligible, and the spreading is the least among the four cases. The characteristics of the screech modes have been addressed in many previous studies, and their effect on jet spreading have been observed in the early experiments of Glass[11] and recently explored further in Ref. 5. In the present paper, attention is first focused on the spreading rate of the jets in the far asymptotic region.

The streamwise variations of mass flux, calculated from data similar to those in Fig. 3, are presented in Fig. 4. The data are nondimensionalized by the initial flux calculated from operating conditions (plenum chamber and ambient), with the assumption of a top-hat velocity profile at the exit of the nozzle. (Direct measurement of the mass flow rate by an orifice-meter, conducted in separate experiments,[5] showed good agreement with the calculated $\dot{m}_e$ data.) The Pitot probe survey was carried out far enough downstream for each case so that the asymptotic region, characterized by a linear variation of $\dot{m}/\dot{m}_e$, was reached. In general, the measurements had to be carried out farther downstream with increasing M_J. An inspection of Fig. 4 reveals that the slopes of the flux curves decrease with increasing M_J.

The asymptotic spreading rates were determined from the slopes of the mass flux curves, measured in the farthest downstream regions. These slopes, measured directly from Fig. 4, are plotted in Fig. 5(a) as a function of M_J. The solid line represents Eq. (4) from the analysis given in the next section. The trend of decreasing asymptotic spreading rate with increasing M_J is clearly exhibited by these data.

Dimensional analysis indicates that the spreading rate should scale as the square-root of the air density at the nozzle exit. Thus, when normalized by $(\rho_a/\rho_e)^{1/2}$ one might expect the rate to become a constant and independent of M_J.[8,12]

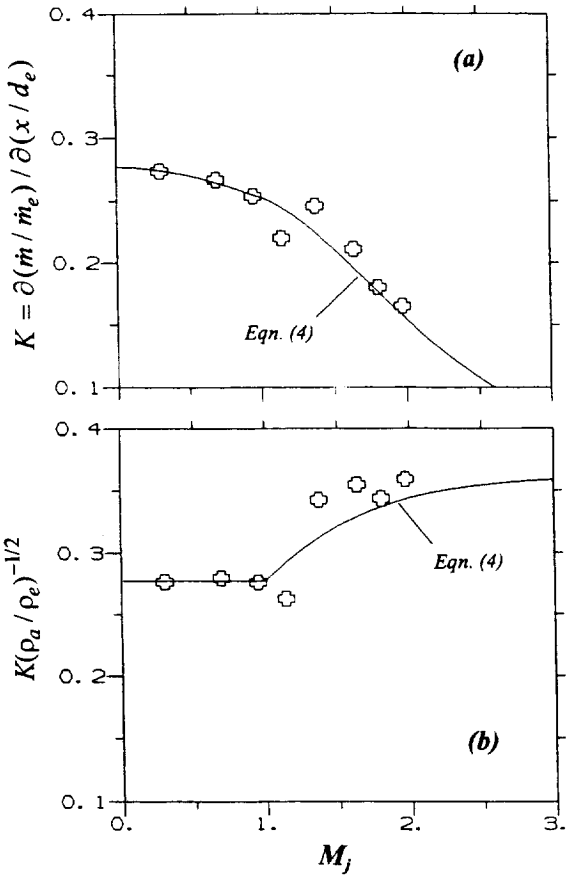

FIG. 5. Asymptotic slopes of $\dot{m}/\dot{m}_e$ versus x/d_e for the convergent nozzle; solid line, Eq. (4). (a) Slopes as measured, (b) normalized slopes.

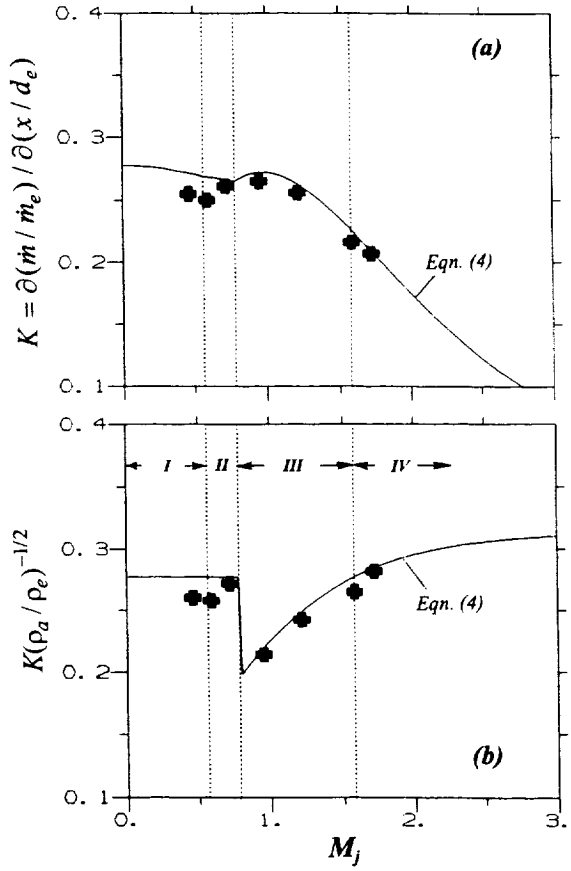

FIG. 6. Data, corresponding to those in Fig. 5, for the convergent-divergent nozzle.

This is examined in Fig. 5(b) where the same data are replotted with such normalization. One finds that the normalized slope is not a constant and varies across the transonic region. It is this "anomalous" behavior that prompted a full investigation with data from the C-D nozzle. Corresponding asymptotic spreading rate data for the C-D nozzle are shown in Figs. 6(a) and 6(b). Here, the flow regimes determined from quasi-one-dimensional flow analysis (see, e.g., Ref. 13), as mentioned in Sec. II, are indicated by the dotted vertical lines. The data in Fig. 6(b) again show that normalization by the square-root of the density ratio does not yield a constant value of the spreading rate. These trends, and the analytical predictions are discussed further in the following sections.

The variations of the centerline velocity for the convergent nozzle are shown in Fig. 7(a) for different M_J. Note that the inverse of U_c, normalized by the nozzle exit velocity (U_e), is plotted. Note furthermore that U_e becomes a constant, equal to the sonic velocity, in regimes III and IV (for $M_J > 1$ with the convergent nozzle). Clearly, the asymptotic slopes decrease with increasing M_J. Corresponding centerline velocity variations for the C-D nozzle are shown in Fig. 7(b), exhibiting a more complex dependence on M_J.

The asymptotic decay rates of U_c, obtained directly from Fig. 7(a), for the convergent nozzle are shown in Fig. 8(a). Corresponding data for the C-D nozzle are presented in Fig. 8(b). The solid curves in these figures represent the analytical prediction described shortly. As with the spreading rate data in Figs. 5 and 6, normalization by $(\rho_a/\rho_e)^{1/2}$ was investigated for the data of Fig. 8. These results are not shown for brevity and it should suffice to state that the normalization yielded constant slopes only through regimes I and II (up to $M_J = 1$ for the convergent nozzle), and variations occurred in regimes III and IV. The reason for these variations becomes clear from the analysis and discussion in the following sections.

IV. ANALYSIS

It is clear that, for the far asymptotic region ($x \gg d_e$), the spreading rate, K, in $\dot{m}/\dot{m}_e = K(x/d_e)$, decreases with increasing M_J. Similarly, the centerline velocity decay rate C, in, $U_e/U_c = C(x/d_e)$ also decreases with increasing M_J. These trends are analyzed first.

Dimensional analysis provides (see, e.g., Ref. 8)

$$\dot{m} = K_1 \dot{F}^{1/2} \rho_a^{1/2} x, \tag{1}$$

where K_1 is a constant. The asymptotic rate of change of momentum, $\dot{F}$, can be equated with forces at the nozzle exit as

$$\dot{F} = A_e \rho_e U_e^2 + (p_e - p_a) A_e. \tag{2}$$

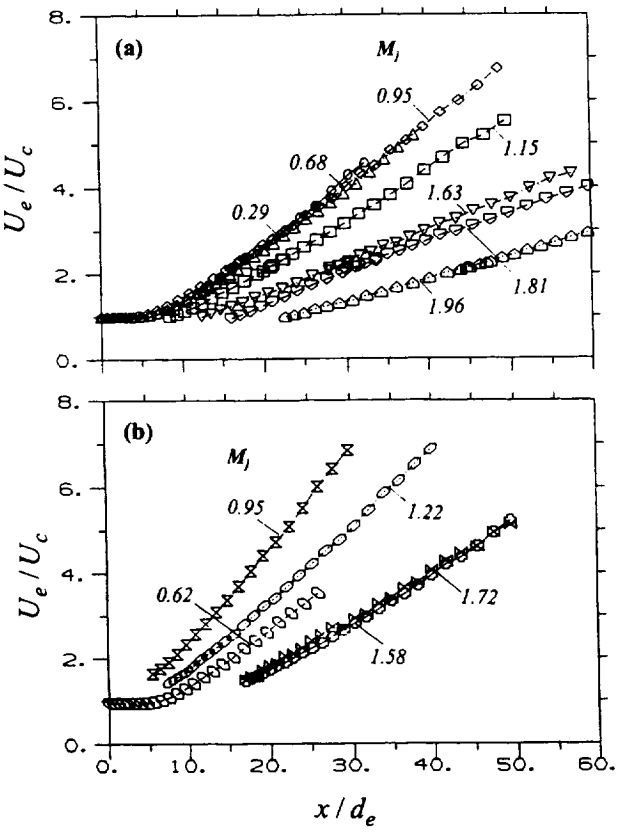

FIG. 7. Streamwise variations of centerline mean velocity (U_c, shown as U_e/U_c) for different M_j; (a) convergent nozzle, (b) convergent-divergent nozzle.

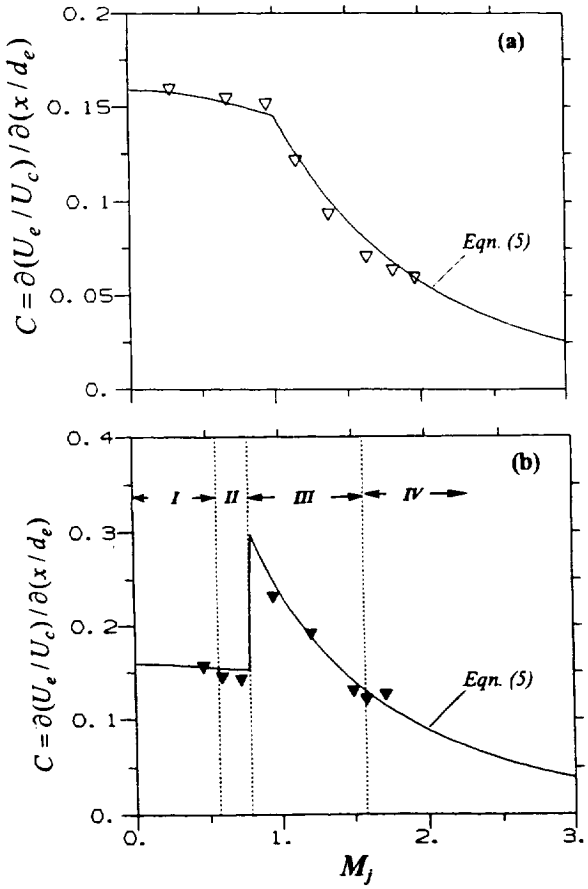

FIG. 8. Asymptotic slopes of U_e/U_c vs x/d_e as a function of M_j; solid line, Eq. (5). (a) Convergent nozzle, (b) convergent-divergent nozzle.

Here, A represents the nozzle cross-sectional area. The subscript "a" represents ambient conditions and "e" represents conditions at the nozzle exit. Let $\dot{F}=\xi A_e\rho_e U_e^2$, so that the "force coefficient," ξ, is given by

$$\xi=1+(p_e-p_a)/\rho_e U_e^2. \tag{3}$$

Substitution in Eq. (1), with $\dot{m}_e=A_e\rho_e U_e$, yields, $\dot{m}/\dot{m}_e=K_1\xi^{1/2}(A_e\rho_e U_e^2)^{1/2}\rho_a^{1/2}x/(A_e\rho_e U_e)$. With $A_e=\pi d_e^2/4$ and $K_2=K_1(4/\pi)^{1/2}$, one obtains

$$\dot{m}/\dot{m}_e=K_2\xi^{1/2}(\rho_a/\rho_e)^{1/2}(x/d_e). \tag{4}$$

In a similar manner, dimensional analysis for the asymptotic variation of centerline velocity yields $U_c=C_1\dot{F}^{1/2}\rho_a^{-1/2}x^{-1}$. One can then obtain

$$U_e/U_c=C_2\xi^{-1/2}(\rho_a/\rho_e)^{1/2}(x/d_e), \tag{5}$$

where C_1 and C_2 are constants. The coefficient on the right of Eq. (4), $(K=K_2\xi^{1/2}(\rho_a/\rho_e)^{1/2})$, as stated earlier, is approximately equal to 0.28 for incompressible jets. Similarly, for incompressible flow, the coefficient on the right of Eq. (5), $(C=C_2\xi^{-1/2}(\rho_a/\rho_e)^{1/2})$, is ~0.16 (present data; see also, Ref. 9). These incompressible constants, i.e., $K_2=0.28$ and $C_2=0.16$, are assumed in the analysis. For compressible jets, one needs to calculate ξ and ρ_e in order to predict the variations of K and C with M_J.

As stated in Sec. II, from one-dimensional nozzle flow analysis, the following flow regimes are expected as the pressure ratio (p_t/p_a), and hence M_J, is increased: (I) Subsonic throughout, (II) normal shock in the divergent section, (III) overexpanded flow, and (IV) underexpanded flow.

A. Calculation of ξ

Through regimes I and II, $p_e=p_a$, therefore, $\xi=1$ [Eq. (3)]. Between regimes II and III (normal shock at the nozzle exit), there is a discontinuity in the variation of p_e, and hence in ξ (discussed further in the following). In regimes III and IV, M_e equals the design Mach number, M_D, and thus, p_e is given by $p_e/p_t=(1+[(\gamma-1)/2]M_D^2)^{-\gamma/(\gamma-1)}$. Since $U_e=M_D\sqrt{\gamma RT_e}$, ($T$ being the temperature and R the ideal gas constant), Eq. (3) provides, $\xi=1+[1/(\gamma M_D^2)](1-p_a/p_e)$. Thus, ξ is known throughout regimes I–IV.

B. Calculation of ρ_e

In regime I,

$$M_e=\left(((p_t/p_a)^{(\gamma-1)/\gamma}-1)\,\frac{2}{\gamma-1}\right)^{1/2},$$

and in regimes III and IV, $M_e=M_D$. In these regimes ρ_e is given by, $\rho_e/\rho_t=[1+[(\gamma-1)/2]M_e^2]^{-1/(\gamma-1)})$, where $\rho_t=p_t/RT_t$. For regime II (normal shock within the diverging section), conditions at the nozzle exit for a given p_t/p_a are found by iteration. With standard compressible flow notations (see, e.g., Ref. 13), the mass flow rate for choked flow, $\dot{m}^*=0532A^*p_t/\sqrt{T_t}$ (foot-pound-second units), is calcu-

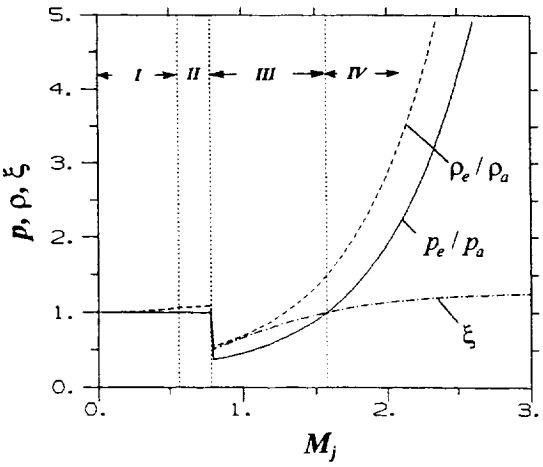

FIG. 9. For the convergent-divergent nozzle, ideal variations of p_e, ρ_e, and ξ with M_j.

lated. Assuming the normal shock at a location where the nozzle cross-sectional area is A, M_1 (Mach number upstream of normal shock) is found from

$$\left(\frac{A}{A^*}\right)^2=\frac{1}{M_1^2}\left[\frac{2}{\gamma+1}\left(1+\frac{\gamma-1}{2}M_1^2\right)\right]^{(\gamma+1)/(\gamma-1)}.$$

From,

$$\frac{p_{t2}}{p_{t1}}=\left[\frac{(\gamma+1)M_1^2}{(\gamma-1)M_1^2+2}\right]^{\gamma/(\gamma-1)}\left[\frac{\gamma+1}{2\gamma M_1^2-(\gamma-1)}\right]^{1/(\gamma-1)},$$

with $p_{t1}=p_t$, p_{t2} is found. This in turn provides M_e from,

$$M_e=\left(((p_{t2}/p_a)^{(\gamma-1)/\gamma}-1)\frac{2}{\gamma-1}\right)^{1/2}.$$

Then T_e is found, with $T_t=T_{t1}=T_{t2}$, from, $T_e/T_t=(1+[(\gamma-1)/2]M_e^2)^{-1}$. Equations, $U_e=M_e\sqrt{\gamma RT_e}$ and $\rho_e=p_a/RT_e$, provide U_e and ρ_e. Finally, iteration is done by varying A until $\dot{m}^*=A_e\rho_eU_e$ is satisfied. This provides shock location as well as conditions at the nozzle exit including ρ_e. Thus, ρ_e is found throughout regimes I–IV. Variations of ρ_e, ξ as well as p_e for the C-D nozzle are shown in Fig. 9. These are discussed further in Sec. V.

C. Potential core length

From the centerline velocity data shown in Fig. 7, a "virtual origin" can be defined by extrapolating the asymptotic straight line upstream and finding its intersection with the $U_e/U_c=1$ line. The distance of the virtual origin from the nozzle (x_c) would also provide a measure of the potential core length (x_p) of the jets. The latter length denotes the distance from the nozzle where the centerline velocity begins to decay. Normally, x_c would be larger than x_p, since it would take some distance, after the decay of U_c has started, for the asymptotic linear variation to ensue. The length x_c can be formally expressed starting with Eq. (5), by assigning a fixed value of unity for the left hand side. Thus, with $D_2=1/C_2$, an expression for x_c is obtained as

$$x_c/d_e=D_2\xi^{1/2}(\rho_a/\rho_e)^{-1/2}. \tag{6}$$

As with Eqs. (4) and (5), an incompressible constant is assumed for the right hand side of Eq. (6). From the data for the lowest subsonic case in Fig. 7(a), this constant is assumed to be seven. That is, $D\ (=D_2\xi^{1/2}(\rho_a/\rho_e)^{-1/2})$ is taken as $7d_e$ for incompressible flow. Note that the potential core length for incompressible jets is about $4d_e$, but, as stated in the foregoing, the distance of the virtual origin is somewhat longer. The same calculations of ξ and ρ_e, described previously, would then provide the variation of x_c/d_e with M_j in the compressible flow regime.

V. DISCUSSION

The analytical curves in Figs. 5 and 6 represent Eq. (4). The value of the slope has been matched on the left end of the graphs with $K=0.28$. This is the approximate value of the slope observed in previous experiments.[6,9] This is the only matching that has been done in the present analysis, the rest following from compressible flow equations. The agreement with the data is quite good. A similar observation can be made for the centerline velocity decay rates in Fig. 8. Good comparison is observed with the predictions from Eq. (5).

Inspecting the expression for ξ and Eq. (4), it should be apparent that the value of the slope, $K_2\xi^{1/2}$ $(=K(\rho_a/\rho_e)^{-1/2})$, for a convergent nozzle should be 0.28 up to $M_j=1$ ($\xi=1$ in that range and $K_2=0.28$). In the limit of large M_j, it should reach a value of 0.367 (with $\gamma=1.4$). The trend is approximately followed by the data [Fig. 5(b)]. For a C-D nozzle, $K_2\xi^{1/2}$ should be 0.28 up to the point when the normal shock leaves the nozzle (demarcation between regimes II and III), and again attain the same magnitude at M_D (demarcation between regimes III and IV). In the overexpanded regime its value should be lower than the incompressible constant, since $p_e<p_a$. In the limit of large M_j, for underexpanded flow, its value should be lower than the corresponding value for a convergent nozzle, and depend on M_D. These trends are also qualitatively in agreement with the data presented in Fig. 6(b).

The discontinuity in the predicted trends between regimes II and III is due to the assumptions in the one-dimensional nozzle flow analysis. There occurs a discontinuity in the total pressure variation across the normal shock [Figs. 2(b) and 9]. In the analysis, for regime II, it is assumed that the total pressure upstream of the shock equals the plenum chamber pressure. Downstream of the shock, the flow becomes subsonic and the pressure drops to a value such that the static pressure at the nozzle exit equals p_a. Thus, up to the end of regime II, $p_e=p_a$. As the shock leaves the nozzle exit, the total pressure at the exit goes through a discontinuous variation, attaining the value that was upstream of the shock. The Mach number at the nozzle exit also jumps to the design Mach number and remains the same throughout regimes III and IV. The static pressure at the nozzle exit, given by the compressible flow equations discussed in the previous section, is at first low in the overexpanded regime. With increase in plenum chamber pressure, it increases and exceeds ambient pressure when the flow becomes underexpanded. This idealized variation of p_e for the given C-D

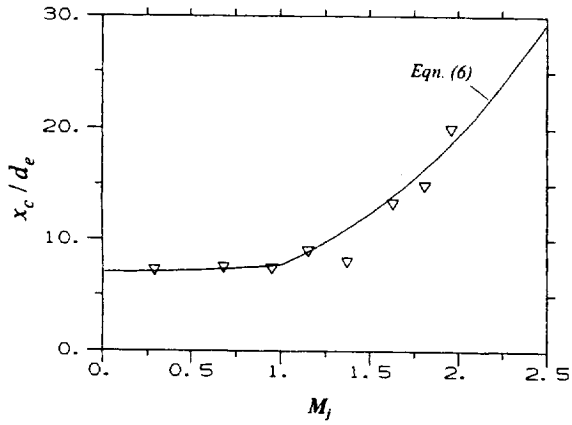

FIG. 10. Distance of "virtual origin location" vs M_j for the convergent nozzle; solid line, Eq. (6).

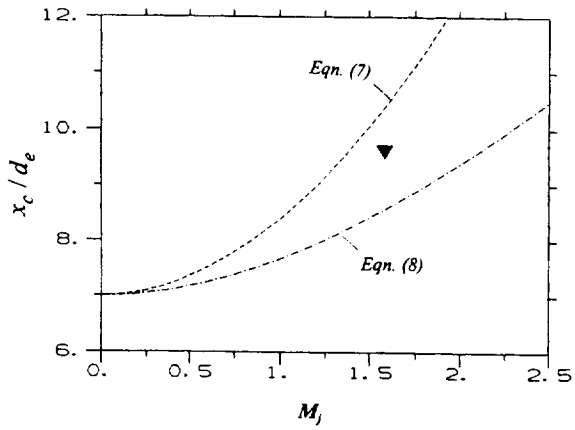

FIG. 11. Distance of "virtual origin location" vs M_j for fully expanded jets. Symbol: Present data from the convergent-divergent nozzle; Eq. (7): Correlation due to Professor C. K. W. Tam based on data from Refs. 18 and 19; Eq. (8): Effect of ρ_e on x_c, present analysis.

nozzle can be seen in Fig. 9. It can also be seen in Fig. 9 that the corresponding variations of ρ_e and ξ similarly go through discontinuities at the end of regime II. The discontinuities in ξ and ρ_e result in discontinuities in the predictions. In the actual flow, however, such a sharp discontinuity is not possible. The shock would not remain normal as it approached the nozzle exit. There would be unsteadiness. As a result the sharp variations would be smoothed out. However, this issue concerns only a narrow range of M_j between regimes II and III and is not relevant for the rest of the discussion.

The reason why normalization by $(\rho_a/\rho_e)^{1/2}$ does not yield a constant value of the slopes (i.e., constant $K_2\xi^{1/2}$ or $C_2\xi^{-1/2}$) at all M_j should also be apparent by now. A constant value of these slopes would be expected only for subsonic and fully expanded supersonic conditions. For imperfectly expanded conditions the pressure term appears in the momentum balance equation, resulting in a value of ξ that is different from unity. This causes the observed deviations. It should also be obvious that proper normalization would be achieved only when the term ξ is also taken into account in addition to the density ratio. Specifically, a constant value of the slopes would be obtained when K is normalized by $\xi^{1/2}(\rho_a/\rho_e)^{1/2}$ and C is normalized by $\xi^{-1/2}(\rho_a/\rho_e)^{1/2}$. In passing, it should be noted that the assumption, $p_e=p_a$, does not strictly hold even for incompressible jets (see Refs. 9, 14, and 15). However, the effect of the deviations in p_e for that regime is already included in the incompressible constants ($K_2=0.28$ and $C_2=0.16$) assumed in the analysis.

Now, let us compare the prediction from Eq. (6) with the data. This is shown in Fig. 10 for the convergent nozzle. A few points should be emphasized before further discussion. First, the "potential core length," x_p, for a convergent nozzle is not well-defined in the supersonic regime. The velocity at the nozzle exit (U_e) is sonic. This is less than the velocity that would have occurred if the flow expanded fully. As the underexpanded supersonic flow negotiates the shock-expansion structure downstream, there should be an overall increase in the centerline velocity U_c before a decrease by turbulent diffusion ensues. This alone would explain an increasingly longer potential core with increasing M_j. The virtual origin location, x_c, however, is a clearly defined quantity. It is defined the same way in the experiment and the analysis, and, therefore, the comparison is meaningful. However, x_c is unlikely to represent x_p in a consistent manner (say, being larger by the same ratio) throughout all flow regimes. Second, the analysis pertains to the asymptotic region where self-similarity has been achieved. The domain up to the virtual origin, however, is characteristic of the developing region that is affected by many parameters such as initial condition, nozzle shape, occurrence of screech, etc. Another factor that comes into play is the well-known compressibility effect that reduces turbulent mixing efficiency.[16,17] Reduced turbulent mixing with increasing jet Mach number is a factor commonly thought to result in a longer potential core. Finally, in continuation of the second point, note that there is nothing in Eq. (6) to account for the variation of mixing efficiency in the developing region. The analysis does not "know" what has happened in the developing region that may have affected the length of the potential core. Inspecting the derivation leading to Eq. (6), it should be clear that x_c is simply the intercept of the asymptotic straight line, passing through the origin, with the $U_e/U_c=1$ line. The length of this intercept depends on the asymptotic slope that in turn depends solely on the density and static pressure at the nozzle exit.

Yet, it can be seen in Fig. 10 that the data fall close to the prediction. This is thought to be a coincidence. Here, the jet is subjected to conflicting effects. A reduced mixing efficiency with increasing M_j tends to elongate the potential core. But screech, occurring with this nozzle in the supersonic regime, tends to reduce the potential core. Thus, there is a cancellation, and only the effect of the exit conditions has prevailed.

The role played by reduced mixing efficiency with increasing compressibility is now explored further. Data for fully expanded flow are compared in Fig. 11. Only one such data point is available from the C-D nozzle of the present experiment. This is shown by the solid triangular data point. Additional data from the literature are represented by the curve marked Eq. (7). The latter warrants explanation.

Potential core length for fully expanded jets has been

measured, among others, by Lau *et al.*[18] and Lau.[19] Correlation, $x_p/d_e=4.2+1.1M_e^2$, was observed to represent the data in Ref. 18. This correlation was modified, based on additional data from Ref. 19, by Professor C. K. W. Tam (private communication, see also Ref. 20), as follows:

$$x_p/d_e=4.3+1.2M_e^2+f(T_e/T_a),$$

where $f(T_e/T_a)=1.2(1-T_e/T_a)$ for $T_e/T_a\leq 1.0$, and $f(T_e/T_a)=\exp(-3.2(T_e/T_a-1))-1.0$ otherwise. In order to compare with the present analysis, the constant on the right is substituted to obtain the virtual origin location (x_c) as

$$x_c/d_e=7.0+1.2M_e^2+f(T_e/T_a). \tag{7}$$

Thus, the curve on the top of Fig. 11, marked Eq. (7), represents x_c inferred from the experimental results of Refs. 18 and 19. The data point from the present experiment falls somewhat lower. This could be due to a number of factors. The flow with the present nozzle, as mentioned earlier, was not perfectly expanded and there was some residual screech. However, this difference is not important in the context of the present discussion and may be ignored.

The prediction of x_c from the present analysis, for fully expanded flow, follows from Eq. (6). With $\xi=1$, one can write

$x_c/d_e=D_2(\rho_a/\rho_e)^{-1/2}$, which reduces to

$$x_c/d_e=7.0\left(1+\frac{\gamma-1}{2}M_e^2\right)^{1/2}, \tag{8}$$

where the substitution for the incompressible constant has been made. Prediction from Eq. (8) is also shown in Fig. 11. In comparing the two curves in Fig. 11, again, it should be borne in mind that Eq. (7) represents correlation for x_c based on experimental data, whereas Eq. (8) is prediction taking only the conditions at the nozzle exit into account. Equation (8) does not account for events in the developing region that also affect x_c. It should also be emphasized that the curve predicted by Eq. (6) in Fig. 10 applies to a given nozzle, whereas Eq. (8) in Fig. 11 applies to fully expanded flow that would be obtained by different nozzles at different Mach numbers.

It is apparent, from the curve representing Eq. (8) in Fig. 11, that only density variation at the nozzle exit already causes an increase in potential core length with increasing jet Mach number. There is no unbalanced pressure term here. Effect of other factors that influence the developing region (nozzle shape, screech, etc.) are also minimal. At fully expanded conditions screech should be absent, and these results pertain to round nozzles. The factor that is still operative affecting the developing region is the reduction in mixing efficiency with increasing Mach number. Note that while Eq. (8) predicts a certain lengthening of x_c at a given M_J, the data [Eq. (7)] are consistently larger. It is reasonable to infer that the additional increase in the potential core length, i.e., the difference between Eqs. (7) and (8), is mainly due to the compressibility effect. If Eq. (8) is expanded for moderate M_J, one obtains, $x_c/d_e\approx 7.0+0.7M_e^2$. Thus, for cold jets, the effect of reduced mixing efficiency with increased compressibility can be viewed as essentially an increase in the coefficient of the second term on the right of Eq. (7), from 0.7 to 1.2.

We conclude by observing, once again, that the potential core length increases with increasing jet Mach number not only due to the compressibility effect that reduces turbulent mixing, but also simply due to changes in pressure and density at the nozzle exit. It should also be apparent that the contribution from the unbalanced pressure term can be quite pronounced for imperfectly expanded flows. Note the difference in the ordinate scale between Figs. 10 and 11. The predicted values of x_c/d_e at $M_J=2$, for example, are about 20 and 9 in Figs. 10 and 11, respectively. This difference is due to the occurrence of a high pressure at the nozzle exit when the flow is underexpanded. With overexpanded flow, on the other hand, the effect would be reversed since the unbalanced pressure term is negative, i.e., x_c would be less compared to that in the fully expanded case. This can be easily discerned from the data presented in Fig. 7(b).

VI. CONCLUSION

Asymptotic spreading rates and centerline velocity decay rates for compressible jets are examined in this paper. When these rates are nondimensionalized by the scales occurring at the nozzle exit, following usual practice, a decrease in the rates is observed with increasing jet Mach number. The variation of static pressure and density at the nozzle exit with varying pressure ratio explains these trends quite well. Those variations also partially account for the well-known phenomenon of a lengthening of the potential core with increasing jet Mach number. A decrease in mixing efficiency with increasing compressibility also contributes to, but is not the main reason for, the observed lengthening of the jet potential core.

ACKNOWLEDGMENTS

Thanks are due to Professor Mo Samimy of Ohio State University for reviewing the derivations, to Dr. Jay Panda for providing input on the *C-D* nozzle characteristics, to Dr. Judith Foss Van-Zante for help with some of the data acquisition, and to John M. Abbott for reviewing the manuscript.

[1]K. K. Ahuja and W. H. Brown, "Shear flow control by mechanical tabs," AIAA Paper No. 89-0994, 1989.
[2]K. B. M. Q. Zaman, M. F. Reeder, and M. Samimy, "Control of an axisymmetric jet using vortex generators," Phys. Fluids **6**, 778 (1994).
[3]E. J. Gutmark and F. F. Grinstein, "Passive combustion enhancement using non-circular jets—a review," AIAA paper No. 97-0465, 35th Aerospace sciences Meeting, Reno, Nevada, Jan. 6–10, 1997.
[4]K. B. M. Q. Zaman, "Axis switching and spreading of an asymmetric jet: the role of coherent structure dynamics," J. Fluid Mech. **316**, 1 (1996).
[5]K. B. M. Q. Zaman, "Spreading characteristics and thrust of jets from asymmetric nozzles," AIAA Paper No. 96-0200, 34th Aerospace Sciences Meeting, Reno, Nevada, Jan. 15–18, 1996.
[6]S. C. Crow and F. H. Champagne, "Orderly structures in jet turbulence," J. Fluid Mech. **48**, 547 (1971).
[7]K. B. M. Q. Zaman and G. Raman, "Reversal in spreading of a tabbed circular jet under controlled excitation," Phys. Fluids **9**, 3733 (1997).
[8]F. P. Ricou and D. B. Spalding, "Measurements of entrainment by axisymmetrical turbulent jets," J. Fluid Mech. **11**, 21 (1961).

[9]K. B. M. Q. Zaman, "Flow field and near and far sound field of a subsonic jet," J. Sound Vib. **106**, 1 (1986).

[10]K. B. M. Q. Zaman, "Characterization of asymptotic entrainment rate for compressible jets," AIAA Paper No. 98-0694, 36th Aerospace Sciences Meeting, Reno, Nevada, Jan. 12–15, 1998.

[11]D. R. Glass, "Effects of acoustic feedback on the spread and decay of supersonic jets," AIAA J. **6**, 1890 (1968).

[12]P. O. Witze, "Centerline velocity decay of compressible free jets," AIAA J. **12**, 417 (1974).

[13]A. H. Shapiro, *The Dynamics and Thermodynamics of Compressible Fluid Flow* (The Ronald Press Co., New York, 1953).

[14]A. K. M. F. Hussain and A. R. Clark, "Upstream influence on the near field of a plane turbulent jet," Phys. Fluids **20**, 1416 (1977).

[15]M. T. Islam and M. A. T. Ali, "Mean velocity and static pressure distributions of a circular jet," AIAA J. **35**, 196 (1997).

[16]D. Papamoschou and A. Roshko, "The compressible turbulent mixing layer: an experimental study," J. Fluid Mech. **197**, 453 (1988).

[17]M. Samimy and G. S. Elliott, "Effects of compressibility on the characteristics of free shear layers," AIAA J. **28**, 439 (1990).

[18]J. C. Lau, P. J. Morris, and M. J. Fisher, "Measurements in subsonic and supersonic free jets using a laser velocimeter," J. Fluid Mech. **93**, 1 (1979).

[19]J. C. Lau, "Effects of exit Mach number and temperature on mean-flow and turbulence characteristics in round jets," J. Fluid Mech. **105**, 193 (1981).

[20]A. T. Thies and C. K. W. Tam, "Computation of turbulent axisymmetric and nonaxisymmetric jet flows using the k-ϵ model," AIAA J. **34**, 309 (1996).

-1 5/11/99

TECHNICAL PUBLICATION APPROVAL FORM

AUTHOR(S) *(Continue in Remarks.)*	ORG. CODE	AFFILIATION *(See page 2.)*	PHONE NO.	MAIL STOP	ROOM NO.
KHAIRUL ZAMAN	5860		x5925	5-11	257

Funding Division No. _____ Current Funded Task No. YOM 5122 Funding RTOP No. 522-31-23

Lewis Contract Monitor _____ Org. Code _____ Phone No. _____ Mail Stop _____ Room No. _____

Contract or Grant No. _____ Other Report No. _____ Non-NASA Funding *(Specify)* _____

Contract Organization and Complete Address _____

(1) REPORT TITLE AND SUBTITLE
ASYMPTOTIC SPREADING RATE OF INITIALLY COMPRESSIBLE JETS – EXPERIMENT AND ANALYSIS

(2) REPORT TYPE *(See Page 2 and NPG 2200.2A)*
- ☐ TP
- ☐ TM
- ☐ CR
- ☐ CP
- ☐ SP
- ☐ Informal STI *(Write URL in Remarks.)*
- ☐ Presentation
- ☐ TM or CR
- ☐ No TM or CR *(including oral)*
- ☒ Journal article/book

(3) WORK REQUESTED
- ☐ Edit
- ☐ Process
- ☐ Credit only
Attach complete report.

(4) MEETING TITLE, LOCATION, AND DATE
JOURNAL TITLE

PUBLISHER/SPONSOR
THE PHYSICS OF FLUIDS

(5) DISTRIBUTION
☐ Standard ☐ Nonstandard ☐ Local

SECURITY CLASSIFICATION
☐ Unclassified ☐ Confidential ☐ Secret

Patent Notice given to authors: Initials _____ Date ____/____/____

(6) DISTRIBUTION AVAILABILITY CATEGORY *(See NGP 2200.2A)*

No Restriction
- ☐ Publicly available
- ☐ Publicly available SBIR *(attach letter)*

Confidential Commercial
- ☐ Trade secret
  - ☐ Patent ☐ License Agreement
  - ☐ Space Act Agreement (SAA) No. _____
- ☐ Copyrighted
- ☐ SBIR Restricted until ____/____/____

Export Controlled
- ☐ ITAR – USML Category No. _____
- ☐ EAR – ECCN _____
- ☐ LERD

Availability for restricted document
- ☐ U.S. Government Agencies and U.S. Government Agency Contractors Only
- ☐ NASA Contractors and U.S. Government Agencies Only
- ☐ U.S. Government Agencies Only
- ☐ NASA Personnel and NASA Contractors Only
- ☐ NASA Personnel
- ☐ Available Only with Approval of Issuing Office (Program Office or NASA Center)

Limited until ____/____/____ *(if applicable)*

(7) TRADE NAMES USED? ☐ Yes ☐ No

(8) SUBJECT CATEGORY(IES)

(9) SUBJECT TERMS *(From NASA Thesaurus)*
JETS, MIXING LAYERS, TURBULENCE MODELING, COMPRESSIBILITY

Approvals must be complete before your report can be processed.

(10) MANAGEMENT REVIEWS AND APPROVALS

	Initial	Date
Author/Technical Monitor name *(printed)* KHAIRUL ZAMAN	KZ	2/26/98
Branch Chief/Office Head name *(printed)* ~~NED HANNUM~~		
Division Chief name *(printed)* Ned Hannum	NH	2/27/98

Editing waived? ☒ Yes * ☐ No

TECHNICAL REVIEW COMMITTEE *(Required for standard distribution reports.)*

Chair or Reviewer name *(printed)*		
Checker name *(printed)*		
Advisor name *(printed)*		

(11) DISTRIBUTION REVIEWS AND APPROVALS

	Signature	Date
Author/Originator name *(printed)* KHAIRUL ZAMAN	KZ	2/26/98
Branch Chief name *(printed)* ~~NED HANNUM~~		
Division Chief name *(printed)*		
Intellectual Property Officer name *(printed)(if required)*		
Center Export Administrator name *(printed)*		

*REMARKS THIS MANUSCRIPT IS A SLIGHTLY REVISED VERSION OF THE AIAA PAPER #98-0694, FOR WHICH FULL C-22 PROCEDURE WAS COMPLETED. COPY OF THAT C-22 ATTACHED.

http://www.lerc.nasa.gov/WWW/STI/techinfo/c22.htm